

# Persistent Current due to a Screw Dislocation in Weyl Semimetals: Role of One-Dimensional Chiral States

Kentaro Kodama and Yositake Takane

*Department of Quantum Matter, Graduate School of Advanced Sciences of Matter,  
Hiroshima University, Higashihiroshima, Hiroshima 739-8530, Japan*

(Received )

A Weyl semimetal pierced by a screw dislocation accommodates one-dimensional (1D) chiral states along the corresponding dislocation line. As these states propagate in a particular direction determined by their chirality, a persistent current (i.e., charge current in equilibrium) is expected to appear in the interior of the system. To confirm this expectation, we numerically calculate the charge current in a Weyl semimetal in the presence of a screw dislocation. It is shown that a significant charge current is induced by the 1D chiral states near the dislocation. We also analyze the spatial distribution of the charge current focusing on the top and bottom surfaces of the system, at which the screw dislocation is terminated, and give an overview of how the charge current due to the dislocation is converted to that carried by other states near the termination point of the dislocation.

## 1. Introduction

A Weyl semimetal is a three-dimensional topological system with gapless excitations. It possesses a pair of, or pairs of, nondegenerate Dirac cones with opposite chirality.<sup>1–10)</sup> The conduction and valence bands of each Dirac cone conically touch at the point called a Weyl node in the Brillouin zone. A notable feature of a Weyl semimetal is that low-energy chiral states appear on its surface in a two-dimensional (2D) manner<sup>3)</sup> if a pair of Weyl nodes is projected onto two different points in the corresponding surface Brillouin zone. These 2D chiral surface states are collectively referred to as a Fermi arc as they appear to connect a pair of projected Weyl nodes. It has been shown that similar chiral states also appear in a Weyl semimetal in the presence of a screw dislocation (Fig. 1)<sup>11, 12)</sup> or an edge dislocation.<sup>13)</sup> In this case, the chiral states are localized along each dislocation line as those observed in topological insulators;<sup>14–18)</sup> thus, they appear in a one-dimensional (1D) manner. Some materials, such as TaAs and NbAs, have been experimentally identified as Weyl semimetals.<sup>19–26)</sup>

For definiteness, we consider a prototypical Weyl semimetal with a pair of Weyl nodes at  $\mathbf{k}_{\pm} = (0, 0, \pm k_0)$  in reciprocal space and  $E = 0$  in energy space. We assume that the system is in the shape of a prism or cylinder of finite length aligned along the  $z$ -direction. In this case, the 2D chiral surface states appear on the side surface of the system. Let us focus on the 1D chiral states along a screw dislocation parallel to the  $z$ -axis. As the 1D chiral states propagate only in a particular direction determined by their chirality, they collectively carry a charge current in the direction opposite to its propagating direction. This suggests the possibility that a persistent charge current is spontaneously induced in the interior of a Weyl semimetal in equilibrium.

Previously, Sumiyoshi and Fujimoto<sup>27)</sup> analyzed the response of a Weyl semimetal upon the insertion of a screw (or edge) dislocation to answer the question of whether the fictitious magnetic field<sup>28)</sup> due to the dis-

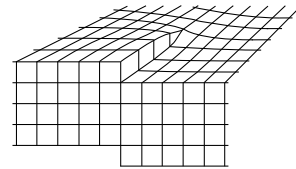


**Fig. 1.** Screw dislocation with a displacement of one unit atomic layer terminated on a top surface.

location gives rise to a local charge current. They found that a local charge current does appear along the dislocation. This phenomenon can be regarded as a chiral magnetic effect in equilibrium, which is forbidden for a uniform magnetic field.<sup>29–37)</sup> However, they did not analyze the case in which 1D chiral states are accommodated near a screw dislocation. That is, the local charge current considered in Ref. 27 is induced by the response of bulk states to the fictitious magnetic field. It is natural to expect that the 1D chiral states more significantly contribute to the local charge current than the bulk states. However, this has not been verified yet. Furthermore, the distribution of charge current has not been explicitly examined in a realistic system of finite size. The charge current in equilibrium must vanish if it is integrated over an entire cross section of singly connected systems. That is, the charge current near the dislocation is canceled out by that near the side surface, which should flow in the opposite direction, as well as by that due to bulk states. This observation gives rise to the natural question: how is the charge current near the dislocation converted to the surface charge current at the top and bottom surfaces?

In this paper, we analyze the local charge current in a Weyl semimetal to answer the question raised above. Using a standard tight-binding model for a Weyl semimetal, which possesses particle-hole symmetry, we calculate the spatial distribution of the charge current in the presence of a screw dislocation. It is shown that the local charge current significantly depends on the location of the Fermi

energy  $E_F$ . If  $E_F$  is at the band center, which corresponds to the energy at the Weyl nodes (i.e.,  $E = 0$ ), the local charge current completely vanishes everywhere in the system even in the presence of a screw dislocation. A finite charge current is observed near the dislocation once  $E_F$  is displaced from the band center. It is clearly shown that the contribution to the charge current from the 1D chiral states significantly dominates that from the bulk states. Indeed, the local charge current becomes significantly small in the absence of the 1D chiral states. It is also shown that the charge current is nearly proportional to  $E_F$  as long as  $E_F$  is located near the band center. We finally examine how the charge current near a screw dislocation is converted to the surface current at the top and bottom surfaces of the system. It is shown that the conversion is mainly mediated through the edge dislocation, which connects the screw dislocation and the side surface.

In the next section, we present a tight-binding model on the cubic lattice for a Weyl semimetal with a pair of Weyl nodes at  $\mathbf{k}_\pm = (0, 0, \pm k_0)$ . It is pointed out that no spontaneous charge current appears in the system if the Fermi energy is located at the band center (i.e.,  $E_F = 0$ ). In Sect. 3, we analyze the low-energy electron states in a cylindrical Weyl semimetal by using a continuum approximation. We clarify the behaviors of the 1D chiral states along a screw dislocation and the 2D chiral states near a side surface. We approximately determine the charge current due to these chiral states at zero temperature. In Sect. 4, we numerically obtain the spatial distribution of the charge current at zero temperature by using the model given in Sect. 2. We treat two particular structures: the system of a rectangular prism with two antiparallel screw dislocations under the periodic boundary condition in the three directions and that of a regular prism with a screw dislocation under the open boundary condition in the three directions. The last section is devoted to a summary. We set  $\hbar = 1$  throughout this paper.

## 2. Model

We introduce a tight-binding model for Weyl semimetals on a cubic lattice with the lattice constant  $a$ , where lattice sites are specified by indices  $l$ ,  $m$ , and  $n$ , respectively, in the  $x$ -,  $y$ -, and  $z$ -directions. The two-component state vector for the  $(l, m, n)$ th site is expressed as

$$|l, m, n\rangle = [ |l, m, n\rangle_\uparrow, |l, m, n\rangle_\downarrow ], \quad (1)$$

where  $\uparrow, \downarrow$  represents the spin degree of freedom. The tight-binding Hamiltonian is given by  $H = H_0 + H_x + H_y + H_z$  with<sup>4,5)</sup>

$$H_0 = \sum_{l,m,n} |l, m, n\rangle h_0 \langle l, m, n|, \quad (2)$$

$$H_x = \sum_{l,m,n} \{ |l+1, m, n\rangle h_x \langle l, m, n| + \text{h.c.} \}, \quad (3)$$

$$H_y = \sum_{l,m,n} \{ |l, m+1, n\rangle h_y \langle l, m, n| + \text{h.c.} \}, \quad (4)$$

$$H_z = \sum_{l,m,n} \{ |l, m, n+1\rangle h_z \langle l, m, n| + \text{h.c.} \}, \quad (5)$$

where

$$h_0 = \begin{bmatrix} 2t \cos(k_0 a) + 4B & 0 \\ 0 & -2t \cos(k_0 a) - 4B \end{bmatrix}, \quad (6)$$

$$h_x = \begin{bmatrix} -B & \frac{i}{2}A \\ \frac{i}{2}A & B \end{bmatrix}, \quad (7)$$

$$h_y = \begin{bmatrix} -B & \frac{1}{2}A \\ -\frac{1}{2}A & B \end{bmatrix}, \quad (8)$$

$$h_z = \begin{bmatrix} -t & 0 \\ 0 & t \end{bmatrix}. \quad (9)$$

From the Fourier transform of  $H$ , we find that the energy dispersion of this model is

$$E = \pm \left\{ [\Delta(k_z) + 2B(2 - \cos(k_x a) - \cos(k_y a))]^2 + A^2(\sin^2(k_x a) + \sin^2(k_y a)) \right\}^{\frac{1}{2}}, \quad (10)$$

where

$$\Delta(k_z) = -2t [\cos(k_z a) - \cos(k_0 a)]. \quad (11)$$

A pair of Weyl nodes appears at  $\mathbf{k}_\pm = (0, 0, \pm k_0)$  with  $E = 0$  for moderate values of the parameters. If the system is in the shape of a prism with its top and bottom surfaces parallel to the  $xy$ -plane, Fermi arc states appear only on the side surfaces.

Now, we introduce a screw dislocation parallel to the  $z$ -axis in our tight-binding model without deforming the lattice structure itself. We assume that the screw dislocation is centered at  $(x_d, y_d)$  with  $x_d = (l_d + \frac{1}{2})a$  and  $y_d = (m_d + \frac{1}{2})a$ , and that it has a displacement of  $N$  unit atomic layers characterized by the Burgers vector  $\mathbf{b} = a(0, 0, N)$ . To take this into account, we consider a half plane (i.e., slip plane) with its edge being identical to the dislocation line [see Fig. 2(a)] and modify the hopping terms in  $H$  across it so that each term connects two different layers in the  $z$ -direction [see Fig. 2(c)]. As an example, let us consider the half plane parallel to the  $xz$ -plane [i.e.,  $y = (m_d + \frac{1}{2})a$ ]. In this case, we reconnect the hopping terms in  $H_y$  for any  $n$  in the region of  $l_d + 1 \leq l$  by performing the following replacement:

$$|l, m_d + 1, n\rangle h_y \langle l, m_d, n| + \text{h.c.} \rightarrow |l, m_d + 1, n + N\rangle h_y \langle l, m_d, n| + \text{h.c.}, \quad (12)$$

which indicates that the site with  $m = m_d$  on the  $n$ th layer is connected to the site with  $m = m_d + 1$  on the  $n + N$ th layer across the half plane. Consequently,  $H_y$  is modified as

$$H_y = \sum_{l_d+1 \leq l, m=m_d, n} \{ |l, m+1, n+N\rangle h_y \langle l, m, n| + \text{h.c.} \} + \sum_{\text{otherwise}} \{ |l, m+1, n\rangle h_y \langle l, m, n| + \text{h.c.} \}. \quad (13)$$

If the system size  $N_z$  in the  $z$ -direction is finite (i.e.,  $1 \leq n \leq N_z$ ), as in realistic situations, the summation over  $n$  should be restricted within  $1 \leq n \leq N_z - N$  in the first term in Eq. (13). This reflects the fact that a straight step edge with height  $N$  appears on the top and bottom surfaces in the region of  $l_d + 1 \leq l$  [see Fig. 2(c)]

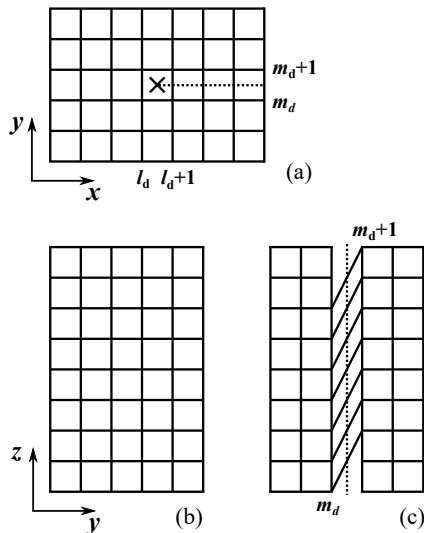


**Fig. 2.** Lattice system in the presence of the screw dislocation with a displacement of two unit atomic layers, where each solid line between two neighboring sites represents a hopping term in  $H_x$ ,  $H_y$ , or  $H_z$  that directly connects the two sites. Dotted lines represent the slip plane across which the hopping terms in  $H$  are modified. (a) Top view with the cross representing the dislocation center. (b) Side view in the unmodified region of  $l \leq l_d$ . (c) Side view in the modified region of  $l_d + 1 \leq l$ .

owing to the presence of the screw dislocation.

We present the charge current operator  $\mathcal{J}_z$  in the  $z$ -direction on the link connecting the  $(l, m, n)$ th and  $(l, m, n + 1)$ th sites. It is given by

$$\mathcal{J}_z = iea[l, m, n + 1]h_z[l, m, n] - \text{h.c.}], \quad (14)$$

which fully describes the charge current in the  $z$ -direction in the absence of a screw dislocation parallel to the  $z$ -axis. In the presence of such a screw dislocation, the tilted hopping term [i.e., the first term of Eq. (13)] also gives rise to the charge current in the  $z$ -direction on the link connecting the  $(l, m_d, n)$ th and  $(l, m_d + 1, n + N)$ th sites only in the region of  $l_d + 1 \leq l$ . This contribution  $\mathcal{J}_z^d$  is expressed as

$$\mathcal{J}_z^d = iea[l, m_d + 1, n + N]h_y[l, m_d, n] - \text{h.c.}]. \quad (15)$$

Assuming the periodic boundary condition in the  $z$ -direction, we give the energy band structures of the system in the two cases considered in Sect. 4: the case with two antiparallel screw dislocations piercing the rectangular cross section [Fig. 3(a)] and that with one screw dislocation piercing the square cross section [Fig. 3(b)]. In the former case with two dislocations, we impose the periodic boundary condition in the  $x$ - and  $y$ -directions to eliminate the side surface, resulting in the absence of 2D chiral states. In the latter case with a single dislocation, the open boundary condition is imposed in the  $x$ - and  $y$ -directions; thus, the 2D chiral states appear near the side surface. The band structures in the two cases are shown in Figs. 4(a) and 4(b) as a function of  $k_z$ , where the area of the cross section  $N_x \times N_y$  is  $24 \times 12$  in the two-dislocation case and  $16 \times 16$  in the one-dislocation case. The following parameters are used:  $B/A = t/A = 0.5$ ,  $k_0a = 3\pi/4$ , and  $N = 2$ . Note that, as we show in the

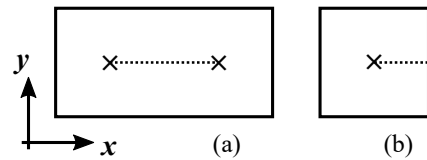


**Fig. 3.** Cross sections of (a) the system with two antiparallel screw dislocations and (b) that with one screw dislocation, where dotted lines represent slip planes.

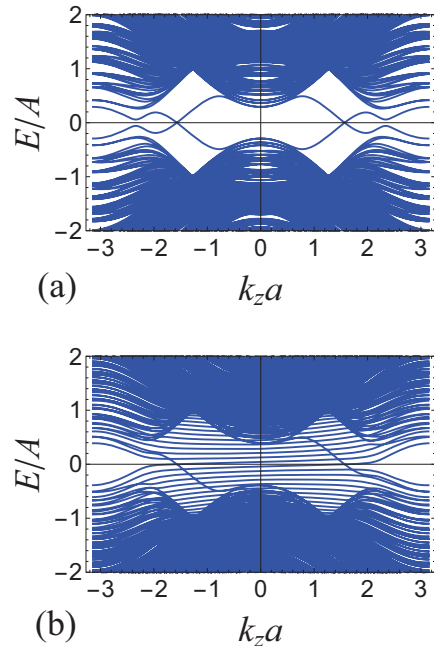


**Fig. 4.** (Color online) Energy dispersions in the (a) two-dislocation case with  $N_x \times N_y = 24 \times 12$  and (b) one-dislocation case with  $N_x \times N_y = 16 \times 16$ .

next section, the 1D chiral states appear in the subgap region of  $-k_0 < k_z < k_0$  such that their branches cross the line of  $E = 0$  at

$$q_l = \frac{2\pi}{Na} \left( -l - \frac{1}{2} \right) \quad (16)$$

satisfying

$$-k_0 < q_l < k_0, \quad (17)$$

where  $l$  is an integer. In the case of  $N = 2$  with  $k_0a = \frac{3\pi}{4}$ , a branch of the 1D chiral states crosses the line of  $E = 0$  at  $k_z a = \frac{\pi}{2}$  or  $-\frac{\pi}{2}$ . This is consistent with the band structures shown in Figs. 4(a) and 4(b). As shown in Fig. 4(b), in the presence of the side surface, the subgap region is filled with many branches with a nearly flat dispersion. These branches represent the 2D chiral surface states. Such branches disappear in the absence of the side surface as clearly seen in Fig. 4(a).

Here, it is important to point out that if  $E_F$  is located at the band center (i.e.,  $E_F = 0$ ), no spontaneous charge current appears in the system described by the model introduced above.<sup>38)</sup> This is directly related to the particle-hole symmetry characterized by the operator  $\Gamma_{\text{ph}}$  defined

by

$$\Gamma_{\text{ph}} = \sigma_x K, \quad (18)$$

where  $\sigma_x$  and  $K$  are respectively the  $x$  component of the Pauli matrices and the complex conjugate operator. The tight-binding Hamiltonian  $H$  satisfies

$$\Gamma_{\text{ph}}^{-1} H \Gamma_{\text{ph}} = -H \quad (19)$$

even in the presence of a screw dislocation. By using this symmetry, we can verify that the local charge current completely vanishes everywhere in the system at  $E_F = 0$ .<sup>38)</sup> This statement relies only on the particle-hole symmetry represented by Eq. (19); thus, it is not restricted to the two-orbital model used in this study and is also applicable to the four-orbital model introduced in Ref. 31 and used in Ref. 27.

### 3. Analysis under a Continuum Approximation

To estimate the magnitude of a charge current, we analyze the 1D chiral states along a screw dislocation and the 2D chiral surface states in a cylindrical Weyl semimetal of radius  $R$  and length  $L_z$ . In this analysis, a continuum approximation<sup>12)</sup> is used under the periodic boundary condition in the  $z$ -direction. The Hamiltonian  $H$  is rewritten in a continuum approximation as

$$H = \begin{bmatrix} \Delta(k_z) + B(\hat{k}_x^2 + \hat{k}_y^2) & A(\hat{k}_x - i\hat{k}_y) \\ A(\hat{k}_x + i\hat{k}_y) & -\Delta(k_z) - B(\hat{k}_x^2 + \hat{k}_y^2) \end{bmatrix}, \quad (20)$$

where  $\hat{k}_x = -i\partial_x$ ,  $\hat{k}_y = -i\partial_y$ . By solving the eigenvalue equation of  $H\Psi = E\Psi$  with  $\Psi(x, y) = {}^t(F, G)$ , we determine the energy dispersion relation of the 1D and 2D chiral states.

It is convenient to use the cylindrical coordinates  $(r, \phi, z)$  with  $r = \sqrt{x^2 + y^2}$  and  $\phi = \arctan(y/x)$ . We assume that a screw dislocation parallel to the  $z$  axis is inserted at  $r = 0$  with a displacement of  $N$  unit atomic layers. We rewrite  $F$  and  $G$  as  $F = e^{il\phi} f(r)$  and  $G = e^{i(l+1)\phi} g(r)$ , where  $l$  is the azimuthal quantum number. The screw dislocation is described by the effective vector potential.<sup>28)</sup>  $e(A_r, A_\phi, A_z) = (0, \zeta(k_z)/r, 0)$  with  $\zeta(k_z) = \frac{Na}{2\pi} k_z$ . As demonstrated in Ref. 12, the eigenvalue equation is decomposed into the two sets of equations:

$$(\mathcal{D}_l - \Lambda_-) f = 0, \quad (\mathcal{D}_{l+1} - \Lambda_-) g = 0 \quad (21)$$

and

$$(\mathcal{D}_l - \Lambda_+) f = 0, \quad (\mathcal{D}_{l+1} - \Lambda_+) g = 0, \quad (22)$$

where

$$\mathcal{D}_l = \partial_r^2 + \frac{1}{r} \partial_r - \frac{(l + \zeta)^2}{r^2}, \quad (23)$$

and  $\Lambda_\pm$  is given by

$$\Lambda_\pm = \frac{A^2 + 2B\Delta \pm \sqrt{(A^2 + 2B\Delta)^2 + 4B^2(E^2 - \Delta^2)}}{2B^2}. \quad (24)$$

Assuming that  $B$  is finite but very small, we can replace

$\Lambda_-$  and  $\Lambda_+$  with

$$\Lambda_- = -\frac{E^2 - \Delta^2}{A^2}, \quad \Lambda_+ = \frac{A^2}{B^2}. \quad (25)$$

The two functions  $f$  and  $g$  are related by the original eigenvalue equation with a very small  $B$ . Hereafter, Eq. (21) with  $\Lambda_-$  and Eq. (22) with  $\Lambda_+$  are respectively referred to as the Weyl equation and supplementary equation. The set of two equations is much more tractable than the original eigenvalue equation.

Let us express an eigenfunction for a given  $l$  as  $\Psi(r) = {}^t(f, g)$ . We require  $\Psi(R) = {}^t(0, 0)$  as a natural boundary condition. In addition,  $\Psi(0) = {}^t(0, 0)$  is also required in the presence of the screw dislocation at  $r = 0$ . We focus on the case of  $|\Delta| > |E|$ , in which the 1D and 2D chiral states appear. In this case, the general solution  $\Psi$  is written as

$$\Psi = c_1 \psi_{l+\zeta}^\eta + d_1 \psi_{l+\zeta}^\kappa + c_2 \psi_{-l-\zeta}^\eta + d_2 \psi_{-l-\zeta}^\kappa, \quad (26)$$

where the functions with  $\eta \equiv \sqrt{\Delta^2 - E^2}/A$  are the solutions of the Weyl equation,

$$\psi_{l+\zeta}^\eta(r) = {}^t[I_{l+\zeta}(\eta r), iR'(E)I_{l+1+\zeta}(\eta r)], \quad (27)$$

$$\psi_{-l-\zeta}^\eta(r) = {}^t[I_{-l-\zeta}(\eta r), iR'(E)I_{-l-1-\zeta}(\eta r)] \quad (28)$$

with  $R'(E) = (-\Delta + E)/\sqrt{\Delta^2 - E^2}$ , and the functions with  $\kappa \equiv A/B$  are the solutions of the supplementary equation,

$$\psi_{l+\zeta}^\kappa(r) = {}^t[I_{l+\zeta}(\kappa r), iI_{l+1+\zeta}(\kappa r)], \quad (29)$$

$$\psi_{-l-\zeta}^\kappa(r) = {}^t[I_{-l-\zeta}(\kappa r), iI_{-l-1-\zeta}(\kappa r)]. \quad (30)$$

Here,  $I_\nu(x)$  is the  $\nu$ th-order modified Bessel function of the first kind. As modified Bessel functions and their linear combinations asymptotically increase or decrease in an exponential manner,  $\Psi$  should describe chiral states spatially localized near  $r = 0$  or  $R$ . The energy dispersion relations of the chiral states are determined by imposing the boundary conditions on  $\Psi$ . See Ref. 12 for details of the derivation.

Now, we present the final result of energy dispersion relations focusing on the low-energy regime of  $E \approx 0$ . Both the 1D and 2D chiral states appear in the limited region of  $-k_0 < k_z < k_0$ , in which  $\Delta(k_z) < 0$ . In this range of  $k_z$ , the low-energy 1D chiral states appear near  $k_z = q_l$  with

$$q_l = \frac{2\pi}{Na} \left( -l - \frac{1}{2} \right). \quad (31)$$

The energy dispersion near  $q_l$  is very steep and is given by

$$E_{1\text{D}}(k_z, l) = -\frac{|\Delta(q_l)|Na}{\pi} \ln \left( \frac{A^2}{B|\Delta(q_l)|} \right) (k_z - q_l). \quad (32)$$

This indicates that a branch of the 1D chiral states appears for each  $l$  satisfying Eq. (17). If  $N = 2$  with  $k_0 a = \frac{3\pi}{4}$ , Eq. (17) is satisfied for  $q_0 a = -\frac{\pi}{2}$  and  $q_{-1} a = \frac{\pi}{2}$ , indicating that the corresponding energy dispersions respectively cross  $E = 0$  at  $k_z = q_0$  and  $q_{-1}$ . If  $N = 1$ , no 1D chiral states appear irrespective of  $k_0$ . In

contrast to the 1D chiral states, the 2D chiral states have a nearly flat dispersion as a function of  $k_z$ . Near  $E = 0$ , their energy dispersion is given by

$$E_{2D}(k_z, l) = \frac{ANa}{2\pi R} (k_z - q_l), \quad (33)$$

where the range of  $k_z$  is limited by  $-k_0 < k_z < k_0$ . This clearly indicates that the energy dispersion becomes completely flat in the absence of a screw dislocation (i.e.,  $N = 0$ ).

Now, we approximately determine the charge current  $I_z$  in the  $z$ -direction at zero temperature, assuming that  $E_F > 0$  for simplicity. As  $I_z$  vanishes at  $E_F = 0$ ,<sup>39)</sup> we are allowed to pick up only the contribution from the energy range of  $0 < E < E_F$ . Let us determine  $I_z^{1D}$  due to the 1D chiral states. The group velocity is

$$v_{1D} = -\frac{|\Delta(q_l)|Na}{\pi} \ln\left(\frac{A^2}{B|\Delta(q_l)|}\right), \quad (34)$$

and the number of  $k_z$  satisfying  $0 < E_{1D}(k_z, l) < E_F$  is given by

$$\text{Number of } k_z = \frac{E_F L_z}{2Na|\Delta(q_l)| \ln\left(\frac{A^2}{B|\Delta(q_l)|}\right)} \quad (35)$$

for each  $l$  satisfying  $-k_0 < q_l < k_0$ . Thus, the charge current due to the 1D chiral states is given by

$$\frac{I_z^{1D}}{L_z} = e \frac{n_{1D} E_F}{2\pi}, \quad (36)$$

where  $n_{1D}$  represents the number of allowed  $l$  (i.e., the number of branches corresponding to the 1D chiral states). For example,  $n_{1D} = 2$  in the case of  $N = 2$  and  $k_0 a = \frac{3\pi}{4}$ . We turn to the contribution from the 2D chiral states. The group velocity in the  $z$ -direction is

$$v_{2D} = \frac{ANa}{2\pi R}, \quad (37)$$

and the numbers of  $k_z$  and  $l$  satisfying  $0 < E_{2D}(k_z, l) < E_F$  are approximately given by

$$\text{Number of } k_z = \frac{k_0 L_z}{\pi} \quad (38)$$

$$\text{Number of } l = \frac{RE_F}{A}. \quad (39)$$

Thus, the charge current due to the 2D chiral states is obtained as

$$\frac{I_z^{2D}}{L_z} = -e \frac{N(k_0 a) E_F}{2\pi^2}. \quad (40)$$

Equations (36) and (40) hold even in the case of  $E_F < 0$ . Although  $I_z^{1D}$  and  $I_z^{2D}$  are determined under the assumption of  $B$  being very small,  $B$  disappears in their final expressions. We thus expect that the resulting  $I_z^{1D}$  and  $I_z^{2D}$  are reliable irrespective of the value of  $B$ . In the case of  $N = 2$  and  $k_0 a = \frac{3\pi}{4}$ , we find that

$$\frac{I_z^{1D}}{L_z} = e \frac{E_F}{\pi}, \quad (41)$$

$$\frac{I_z^{2D}}{L_z} = -e \left(\frac{3}{4}\right) \frac{E_F}{\pi}. \quad (42)$$

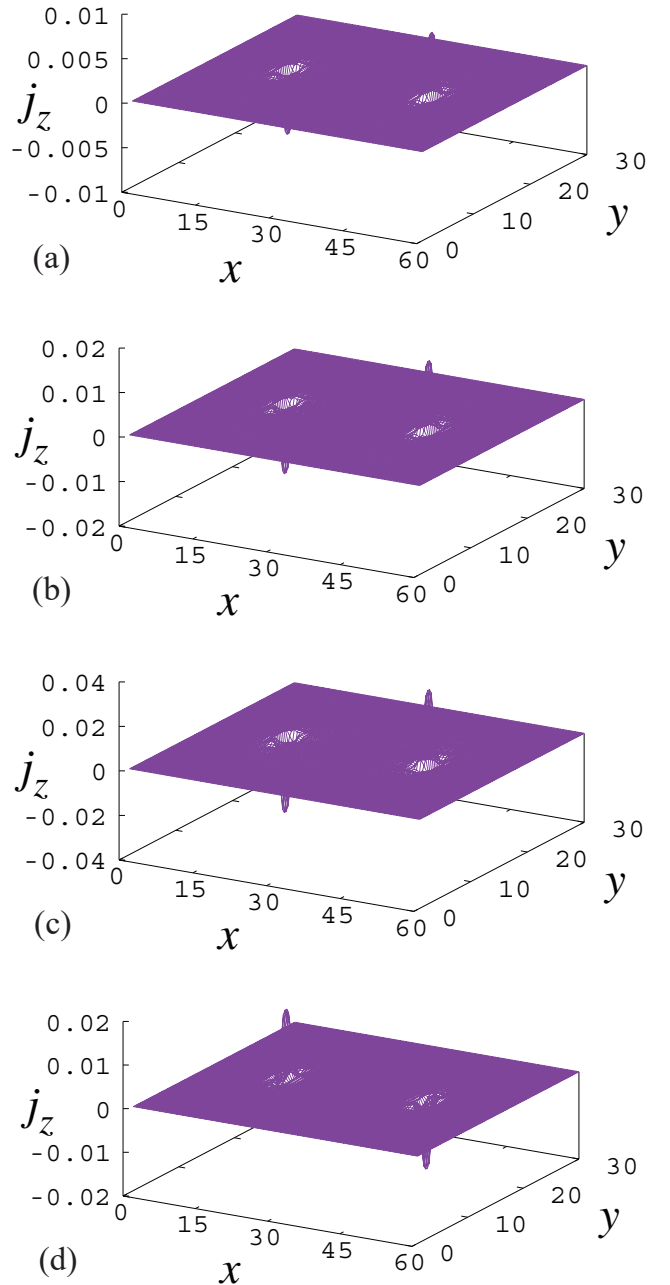


**Fig. 5.** (Color online)  $j_z$  normalized by  $eAN_z a$  in the two-dislocation case with  $N = 2$  on the cross section parallel to the  $xy$ -plane. (a)  $E_F/A = 0.05$ , (b) 0.1, (c) 0.2, and (d)  $-0.1$ . Note that the vertical scale is different from figure to figure.

Generally,  $I_z^{1D}$  and  $I_z^{2D}$  flow in the opposite direction from each other and their magnitude is not identical, leading to the conclusion that the addition of  $I_z^{1D}$  and  $I_z^{2D}$  does not necessarily vanish even after being integrated over a cross section. This means that the bulk states compensate the difference between them.

#### 4. Numerical Results

In this section, we give the numerical results of the local charge current  $j_z$  in the  $z$ -direction and  $j_x$  in the  $x$ -direction at zero temperature. They are obtained by calculating the average of the corresponding operators over the eigenstates with an energy smaller than  $E_F$ . In the two-dislocation case [see Fig. 3(a)], we give  $j_z$  on the

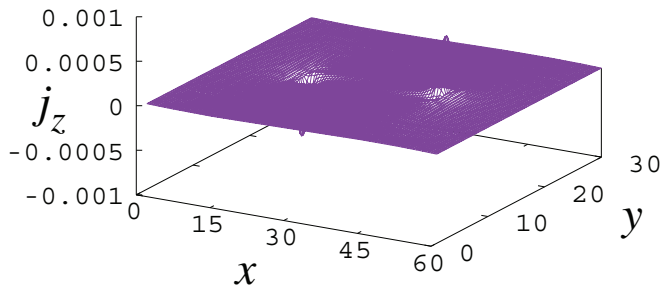


**Fig. 6.** (Color online)  $j_z$  normalized by  $eAN_z a$  in the two-dislocation case with  $N = 1$  on the cross section parallel to the  $xy$ -plane at  $E_F/A = 0.1$ .

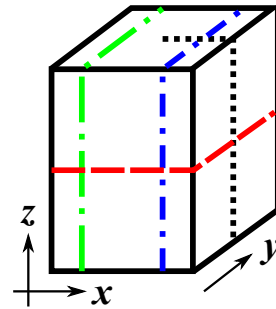
cross section parallel to the  $xy$ -plane to clarify the effect of the 1D chiral states on the persistent current. In the one-dislocation case [see Fig. 3(b)], we give  $j_z$  and  $j_x$  on a few cross sections to observe the spatial distribution of the persistent current in a closed system.

Figure 5 shows  $j_z$  on the cross section parallel to the  $xy$ -plane in the two-dislocation case with  $N = 2$ , where the system of  $N_x \times N_y \times N_z = 60 \times 30 \times 240$  is used in calculating  $j_z$  under the periodic boundary condition in the three directions. In this figure,  $j_z$  is normalized by  $eAN_z a$ . The Fermi energy is located at  $E_F/A = 0.05, 0.1, 0.2$ , and  $-0.1$ , where the result at  $E_F = 0$  is not shown since the local charge current vanishes everywhere in the system. This is consistent with the argument given in Sect. 2. From Figs. 5(a)–5(c), we clearly observe that the magnitude of  $j_z$  is nearly proportional to  $E_F$ , which is consistent with Eq. (36) given in Sect. 3. We also observe that  $j_z$  changes its sign between the result at  $E_F/A = 0.1$  [Fig. 5(b)] and that at  $E_F/A = -0.1$  [Fig. 5(d)] without varying its magnitude. This is also consistent with Eq. (36). As  $j_z$  is positive in the region of  $31 \leq x \leq 60$ , the charge current  $I_z$  in the  $z$ -direction is obtained by integrating  $j_z$  in this region. At  $E_F/A = 0.1$ , the result is

$$\frac{I_z}{L_z} \approx 0.019 \times eA \quad (43)$$

with  $L_z = N_z a$ . This is roughly consistent with Eq. (41). Figure 6 shows  $j_z$  in the two-dislocation case with  $N = 1$  at  $E_F/A = 0.1$ . The 1D chiral states are absent in this case. As clearly seen from Fig. (6), the magnitude of  $j_z$  is much smaller than that in the case with  $N = 2$  at  $E_F/A = 0.1$  [Fig. 5(b)]. This clearly indicates that the 1D chiral states crucially contribute to the persistent current.

We now give the numerical results of  $j_z$  and  $j_x$  in the one-dislocation case with  $N = 2$  on the three cross sections indicated in Fig. 7. In the figures given below,  $j_z$  and  $j_x$  are normalized by  $eAa$ . The open boundary condition is imposed on the system of  $N_x \times N_y \times N_z = 40 \times 40 \times 60$  in the three directions with the Fermi energy fixed at  $E_F/A = 0.1$ . Figure 8(a) shows  $j_z$  on the cross section parallel to the  $xy$ -plane denoted by the dashed (red) line in Fig. 7. The peak structure at the center of the cross section represents the charge current in the  $z$ -direction due to the screw dislocation. In addi-



**Fig. 7.** (Color online) System in a rectangular parallelepiped shape with a screw dislocation in the  $z$ -direction, where the dotted line represents slip plane. In the text, the charge current is considered on the three cross sections denoted by dashed (red), short-dash-dotted (blue), and long-dash-dotted (green) lines.

tion, the charge current in the opposite direction appears near the crossing point between the slip plane and the side surface at  $x = 40$  and  $y = 20$ . This contribution arises from the 2D chiral states circulating around the side surface in a spiral manner. It appears only near the crossing point simply because the screw dislocation is included in our model by modifying only the hopping terms across the slip plane [see Fig. 2(c)]. Figures 8(b) and 8(c) show  $j_x$  on the cross sections parallel to the  $yz$  plane denoted by the short-dash-dotted (blue) and long-dash-dotted (green) lines in Fig. 7. In both figures,  $j_x$  flows in the  $-x$ -direction ( $x$ -direction) near the line edge located at  $y = 1$  ( $y = 40$ ). This represents the charge current due to the 2D chiral states, which circulates around the side surface. In Fig. 8(b), a pair of peak structures is observed near the points at  $y = 20$  on the bottom surface (i.e.,  $z = 1$ ) and on the top surface (i.e.,  $z = 60$ ). As a step edge is located at these points, the two peaks should be identified as the charge current along the edge dislocations on the top and bottom surfaces. Such peak structures do not appear in Fig. 8(b), reflecting the fact that no edge dislocation is present on the corresponding cross section denoted by the long-dash-dotted (green) line in Fig. 7. Figures 8(a)–8(c) indicate that the charge current due to the 1D chiral states is converted to the spiral surface current due to the 2D chiral states mainly through the edge dislocations located at the top and bottom surfaces.

## 5. Summary

We analyzed the local charge current in a Weyl semimetal in the presence of a screw dislocation focusing on the role of 1D chiral states that appear along the corresponding dislocation line. We found several interesting features that were not observed in the previous study.<sup>27)</sup> The most important feature is that the contribution to the charge current from the 1D chiral states significantly dominates that from the bulk states. Another feature is that the local charge current significantly depends on the location of the Fermi energy  $E_F$ . If  $E_F$  is at the band center, the local charge current vanishes everywhere in the system. A finite charge current appears near the dislocation when  $E_F$  is displaced from the band center. The magnitude of the local charge current is nearly propor-

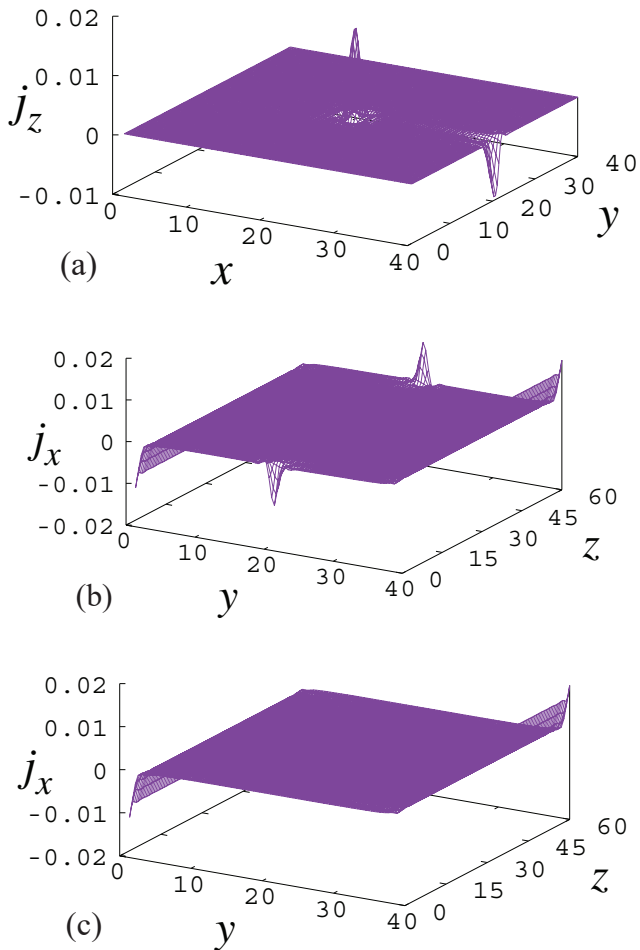


**Fig. 8.** (Color online)  $j_z$  and  $j_x$  normalized by  $eAa$  in the one-dislocation case with  $N = 2$  at  $E_F/A = 0.1$  on the three cross sections denoted in Fig. 7: (a)  $j_z$  on the cross section denoted by the dashed (red) line, (b)  $j_x$  on the cross section denoted by the short-dash-dotted (blue) line, and (c)  $j_x$  on the cross section denoted by the long-dash-dotted (green) line.

tional to  $E_F$  as long as  $E_F$  is located near the band center. We also considered how the charge current due to the 1D chiral states is converted to the surface charge current, as well as the bulk charge current, at the top and bottom surfaces of the system. It is shown that the conversion is mainly mediated through the edge dislocation, which connects the screw dislocation and the side surface.

### Acknowledgment

This work was supported by JSPS KAKENHI Grant Number JP18K03460.

- 1) R. Shindou and N. Nagaosa, Phys. Rev. Lett. **87**, 116801 (2001).
- 2) S. Murakami, New J. Phys. **9**, 356 (2007).
- 3) X. Wan, A. M. Turner, A. Vishwanath, and S. Y. Savrasov, Phys. Rev. B **83**, 205101 (2011).
- 4) K.-Y. Yang, Y.-M. Lu, and Y. Ran, Phys. Rev. B **84**, 075129 (2011).
- 5) A. A. Burkov and L. Balents, Phys. Rev. Lett. **107**, 127205 (2011).

- 6) A. A. Burkov, M. D. Hook, and L. Balents, Phys. Rev. B **84**, 235126 (2011).
- 7) W. Witczak-Krempa and Y. B. Kim, Phys. Rev. B **85**, 045124 (2012).
- 8) P. Delplace, J. Li, and D. Carpentier, Europhys. Lett. **97**, 67004 (2012).
- 9) G. Halász and L. Balents, Phys. Rev. B **85**, 035103 (2012).
- 10) A. Sekine and K. Nomura, J. Phys. Soc. Jpn. **82**, 033702 (2013).
- 11) K.-I. Imura and Y. Takane, Phys. Rev. B **84**, 245415 (2011).
- 12) Y. Takane, J. Phys. Soc. Jpn. **86**, 123708 (2017).
- 13) Y. Takane, J. Phys. Soc. Jpn. **86**, 104709 (2017).
- 14) Y. Ran, Y. Zhang, and A. Vishwanath, Nat. Phys. **5**, 298 (2009).
- 15) Y. Zhang, Y. Ran, and A. Vishwanath, Phys. Rev. B **79**, 245331 (2009).
- 16) K.-I. Imura, Y. Takane, and A. Tanaka, Phys. Rev. B **84**, 035443 (2011).
- 17) Y. Yoshimura, A. Matsumoto, Y. Takane, and K.-I. Imura, Phys. Rev. B **88**, 045408 (2013).
- 18) C. Pauly, B. Rasche, K. Koepf, M. Liebmann, M. Prutzer, M. Richter, J. Kellner, M. Eschbach, B. Kaufmann, L. Plucinski, C. M. Schneider, M. Ruck, J. van den Brink, and M. Morgenstern, Nat. Phys. **11**, 338 (2015).
- 19) H. Weng, C. Fang, Z. Fang, B. A. Bernevig, and X. Dai, Phys. Rev. X **5**, 011029 (2015).
- 20) S.-M. Huang, S.-Y. Xu, I. Belopolski, C.-C. Lee, G. Chang, B. Wang, N. Alidoust, G. Bian, M. Neupane, C. Zhang, S. Jia, A. Bansil, H. Lin, and M. Z. Hasan, Nat. Commun. **6**, 7373 (2015).
- 21) S.-Y. Xu, I. Belopolski, N. Alidoust, M. Neupane, G. Bian, C. Zhang, R. Sankar, G. Chang, Z. Yuan, C.-C. Lee, S.-M. Huang, H. Zheng, J. Ma, D. S. Sanchez, B. Wang, A. Bansil, F. Chou, P. P. Shibayev, H. Lin, S. Jia, and M. Z. Hasan, Science **349**, 613 (2015).
- 22) B.-Q. Lv, H.-M. Weng, B.-B. Fu, X.-P. Wang, H. Miao, J. Ma, P. Richard, X.-C. Huang, L.-X. Zhao, G.-F. Chen, Z. Fang, X. Dai, T. Qian, and H. Ding, Phys. Rev. X **5**, 031013 (2015).
- 23) B. Q. Lv, N. Xu, H. M. Weng, J. Z. Ma, P. Richard, X. C. Huang, L. X. Zhao, G. F. Chen, C. E. Matt, F. Bisti, V. N. Strocov, J. Mesot, Z. Fang, X. Dai, T. Qian, M. Shi, and H. Ding, Nat. Phys. **11**, 724 (2015).
- 24) S.-Y. Xu, N. Alidoust, I. Belopolski, Z. Yuan, G. Bian, T.-R. Chang, H. Zheng, V. N. Strocov, D. S. Sanchez, G. Chang, C. Zhang, D. Mou, Y. Wu, L. Huang, C.-C. Lee, S.-M. Huang, B. Wang, A. Bansil, H.-T. Jeng, T. Neupert, A. Kaminski, H. Lin, S. Jia, and M. Z. Hasan, Nat. Phys. **11**, 748 (2015).
- 25) S. Souma, Z. Wang, H. Kotaka, T. Sato, K. Nakayama, Y. Tanaka, H. Kimizuka, T. Takahashi, K. Yamauchi, T. Oguchi, K. Segawa, and Y. Ando, Phys. Rev. B **93**, 161112 (2016).
- 26) K. Kuroda, T. Tomita, M.-T. Suzuki, C. Bareille, A. A. Nugroho, P. Goswami, M. Ochi, M. Ikhlas, M. Nakayama, S. Akebi, R. Noguchi, R. Ishii, N. Inami, K. Ono, H. Kumigashira, A. Varykhalov, T. Muro, T. Koretsune, R. Arita, S. Shin, T. Kondo, and S. Nakatsuji, Nat. Mater. **16**, 1090 (2017).
- 27) H. Sumiyoshi and S. Fujimoto, Phys. Rev. Lett. **116**, 166601 (2016).
- 28) K. Kawamura, Z. Phys. B **29**, 101 (1978).
- 29) A. A. Zyuzin and A. A. Burkov, Phys. Rev. B **86**, 115133 (2012).
- 30) Y. Chen, S. Wu, and A. A. Burkov, Phys. Rev. B **88**, 125105 (2013).
- 31) M. M. Vazifeh and M. Franz, Phys. Rev. Lett. **111**, 027201 (2013).
- 32) M.-C. Chang and M.-F. Yang, Phys. Rev. B **91**, 115203 (2015).
- 33) M.-C. Chang and M.-F. Yang, Phys. Rev. B **92**, 205201 (2015).
- 34) N. Yamamoto, Phys. Rev. D **92**, 085011 (2015).
- 35) Y. Takane, J. Phys. Soc. Jpn. **85**, 013706 (2016).
- 36) Y. Ibe and H. Sumiyoshi, J. Phys. Soc. Jpn. **86**, 054707 (2017).
- 37) Y. Takane, J. Phys. Soc. Jpn. **88**, 014703 (2019).
- 38) Y. Takane, J. Phys. Soc. Jpn. **87**, 074706 (2018).
- 39) This fact is not taken into consideration in Refs. 12 and 27.